14

SIMPLIFIED MODELS OF INDIVIDUAL NEURONS

In the previous thirteen chapters, we met and described, sometimes in excruciating detail, the constitutive elements making up the neuronal hardware: dendrites, synapses, voltage-dependent conductances, axons, spines and calcium. We saw how, different from electronic circuits in which only very few levels of organization exist, the nervous systems has many tightly interlocking levels of organization that codepend on each other in crucial ways. It is now time to put some of these elements together into a functioning whole, a single nerve cell. With such a single nerve cell model in hand, we can ask functional questions, such as: at what time scale does it operate, what sort of operations can it carry out, and how good is it at encoding information.

We begin this Herculean task by (1) completely neglecting the dendritic tree and (2) replacing the conductance-based description of the spiking process (e.g., the Hodgkin-Huxley equations) by one of two canonical descriptions. These two steps dramatically reduce the complexity of the problem of characterizing the electrical behavior of neurons. Instead of having to solve coupled, nonlinear partial differential equations, we are left with a single ordinary differential equation. Such simplifications allow us to formally treat networks of large numbers of interconnected neurons, as exemplified in the neural network literature, and to simulate their dynamics. Understanding any complex system always entails choosing a level of description that retains key properties of the system while removing those nonessential for the purpose at hand. The study of brains is no exception to this.

Numerous simplified single-cell models have been proposed over the years, yet most of them can be reduced to just one of two forms. These can be distinguished by the form of their output: *spike* or *pulse* models generate discrete, all-or-none impulses. Their output over time can be treated as a series of delta functions $\sum_i \delta(t - t_i)$. Implicitly this assumes that no information is contained in the spike height or width. The original model of a neuron in McCulloch and Pitts (1943) as well as the venerable *integrate-and-fire* unit are instances of pulse models. In *firing rate* neurons, the output is a continuous firing rate, assumed to be a positive, bounded, and stationary function of the input. Examples of these are the units at the heart of Hopfield's (1984) associative memory network.

Yet before we can delve into more detail we need to introduce the deep issue of the proper output representation of a spiking cell, which relates directly to the question of the neuronal code used to transmit information among neurons.

14.1 Rate Codes, Temporal Coding, and All of That

How the neuronal output is represented, as a series of discrete pulses or as a continuous firing rate, relates to the *code* used by the nervous system to transmit information between cells. So let us briefly digress and talk about neuronal codes.

In a typical physiological experiment, the same stimulus is presented multiple times to a neuron and its response is recorded (Fig. 14.1). One immediately notices that the detailed response of the cell changes from trial to trial. Characterizing and analyzing the stochastic components of the neuronal response is important enough that we dedicate the following chapter to it.

Given the pulselike nature of spike trains, the standard procedure to quantify the neuronal response is to count how many spikes arrived within some sampling window Δt and to divide this number by the number of presentations. This yields the conditional probability that a spike occurred between t and $t + \Delta t$ given some particular stimulus.

In the limit of very small sampling windows—such that the probability for more than one spike occurring within Δt is vanishingly small—and infinitely many trials, the probability of spiking is given by $f(t)\delta t$, where $f(t)$ is the *instantaneous firing rate* of the neuron (in units of spikes per time). Plotting $f(t)$ as a function of the time after onset of a stimulus gives rise to the *poststimulus time histogram* (PSTH; Fig. 14.1).

It is important to understand the artificial nature of this construct $f(t)$. The nervous system has to make a decision based on a single spike train and not on the average of tens or more spike trains. A visual neuron in the fly does not have the opportunity to see the hand that is about to swat it approach ten times before it makes the decision to initiate an escape response! A neuron can only observe $\sum_i \delta(t-t_i)$ from its presynaptic partners, and not $f(t)$.

Under certain conditions this might be different. If a cell, say in the cortex, has access to the spiking output of many cells with the same receptive field properties, the temporal average of the single presynaptic neuron can be replaced by an ensemble average over a population of neurons, thereby approximating $f(t)$. In many cases *population rate coding* cannot occur for lack of a sufficient large cell population to average over. In the insect, for instance, a very small number of clearly identifiable neurons code for particular features of the sensory input and no ensemble averaging occurs.

Given the stochastic nature of spike trains, a common assumption is that the averaged firing rate of a neuron constitutes the primary variable relating neuronal response to sensory experience (Adrian and Zotterman, 1926; Adrian, 1932; Lettvin et al., 1959; Barlow, 1972). This belief is supported by the existence of a quantitative relationship between the averaged firing rate of single cortical neurons and psychophysical judgments made by a monkey. That is, the animal's behavior in a visual discrimination task can be statistically predicted by counting spikes over a long interval (typically 1 sec or more) in a single neuron in visual cortex (Werner and Mountcastle, 1963; Barlow et al., 1987; Newsome, Britten, and Movshon, 1989; Vogels and Orban, 1990; Zohary, Hillman, and Hochstein, 1990; Britten et al., 1992).

In these experiments, the rate is estimated by averaging over a window that is large compared to the time in which the sensory stimulus itself changes.

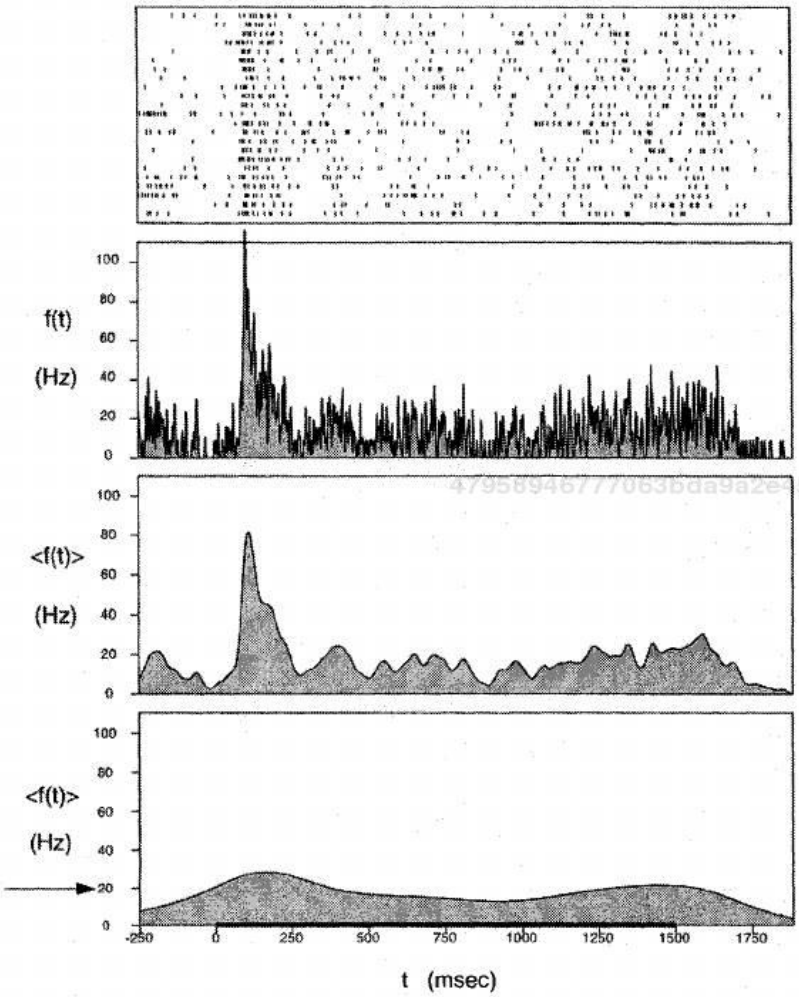

Fig. 14.1 WHAT IS THE FIRING RATE Definition of the *firing rate*. The starting point is numerous trials in which the same stimulus is repeatedly presented to the animal and the spikes generated by some cell are recorded. These are shown in the *raster diagram* at the top, taken from a cell in cortical area V4 in the awake monkey. The stimulus—a grating—is flashed on at 0 and lasts until 1500 msec. Twenty-three of these trials are averaged, smoothed with a Gaussian of 2-msec standard deviation σ and normalized. This averaging window is so small that it effectively defines the instantaneous firing rate $f(t)$. These plots are known as *poststimulus time histograms* (PSTHs). The two lower plots illustrate an *average firing rate* $\langle f(t) \rangle$ obtained from the raster diagrams using Gaussian smoothing with σ set to 20 and 200 msec. In many experiments, only the average number of spikes triggered during each trial, corresponding to a very large value of σ (see arrow at 19.5 Hz), is used to relate the cellular response to the behavior of the animal. It is important to realize that a single neuron only sees spike trains and not a smoothly varying firing rate. Unpublished data from D. Leopold and N. Logothetis, printed with permission.

$$\langle f(t) \rangle = \frac{1}{n} \sum_{j=1}^{n} \frac{1}{\Delta T} \int_{t}^{t+\Delta T} \sum_{i=1}^{n_j} \delta(t' - t_{ij}) dt' \tag{14.1}$$

where the first sum j is executed over the n identical trials and the second sum over all n_j spikes at time t_{ij} during the jth trial. Notice that the δ terms have the dimension of spikes

per δt, so that the average $\langle f(t)\rangle^1$ has the correct units associated with a rate. Instead of a rectangular window, a frequent alternative is smoothing the spike train using a Gaussian convolution kernel with standard deviation σ,

$$\langle f(t)\rangle = \frac{1}{n}\sum_{j=1}^{n}\frac{1}{\sigma\sqrt{2\pi}}\int_{-\infty}^{+\infty} e^{-\frac{(t-t')^2}{2\sigma^2}}\sum_{i=1}^{n_j}\delta(t'-t_{ij})dt' \tag{14.2}$$

(Fig. 14.1). Because of the success in linking $\langle f(t)\rangle$ with behavior, it has been assumed by some that only the mean rate, averaged over a significant fraction of a second or longer, is the relevant code in the nervous system and that the detailed time course of spikes is not.

The past decade has witnessed a revival in the question to what extent an average rate coding neglects information. (For an expose of these ideas, see the superb textbook by Rieke et al., 1996.) On the basis of signal-processing and information-theoretical approaches, we know that individual motion-selective cells in the fly (Bialek et al., 1991), single afferent axons in the auditory system in the bullfrog (Rieke, Warland, and Bialek, 1993) and single neurons in the electrosensory system in weakly electric fish (Wessel, Koch, and Gabbiani, 1996) can carry between 1 and 3 bits of sensory information per spike, amounting to rates of up to 300 bits per second. This information is encoded using the instantaneous rate with a resolution of 5 msec or less. And the elegant experiments of Markram and his colleagues (1997), demonstrating the effect a short delay between a presynaptic and a postsynaptic spike arriving at a synapse can have on its weight (Sec. 13.5.4), provide a biophysical rationale for why timing at the 10 msec level is crucial for synaptic plasticity.

We summarize this vast body of work (see Rieke et al., 1996) by concluding that in many instances $\langle f(t)\rangle$—averaged over a 5–10 msec time frame—appears to be the relevant code used to transmit information:

More complex neuronal codes do exist and are frequently referred to under the catchall term of *temporal coding*. (For an exhaustive listing of possible codes, see Perkel and Bullock, 1968.) However, because of the implication that rate codes do not preserve detailed timing information, we prefer the term coined by Larry Abbott (personal communication), *correlation coding*.

In an instantaneous firing rate code, the generation of each spike is independent of other spikes in the trains (neglecting the refractory period and bursting), only a single number, the rate matters. In a correlation code this assumption is abandoned in favor of coupling among pairs, triplets, or higher order groupings of spikes.

To give one example of a correlation code, let $f(t)$ in response to some stimulus be a maintained response. We assume that this cell is very noisy with distinct spike patterns on individual trials. Averaging over them all leads to a flat response of amplitude f_c. In a rate code, f_c is the only information available to a postsynaptic neuron. Closer inspection of the microstructure of spiking reveals that the intervals between consecutive spikes are not independent of each other, but that two short spike intervals are always followed by a long one. Any code that fails to exploit these higher order correlations among four consecutive spikes would miss something. For experimental evidence of such codes see the references (Segundo et al., 1963; Chung, Raymond, and Lettvin, 1970; Optican and Richmond, 1987; Eskandar, Richmond, and Optican, 1992; Richmond and Optican, 1992).

A generic problem with the assumption of correlation codes is the question of decoding. It is unclear what sort of biophysical mechanisms are required to exploit the information

1. Sometimes also written as $\langle f(t)\rangle_T$ to express its dependency on the size of the averaging window.

hidden in such correlations among spikes. They might be prohibitively complicated to implement at the membrane level.

So far we have said little about *population coding*. Once again, one can distinguish two broad types of codes, correlated ones and noncorrelated ones (Abbott, 1994). The latter are straightforward: here the information from numerous neurons is combined into a population code but without taking account of any correlations among neurons (Knight, 1972a,b). There is plenty of good evidence for such codes in a great variety of different sensory and motor systems, ranging from the four cricket cercal interneurons encoding the direction the wind is blowing from (Theunissen and Miller, 1991) to the larger ensembles encoding the direction of sound in the barn owl (Knudsen, du Lac, and Esterly, 1987; Konishi, 1992) and eye movements in the mammalian superior colliculus (Lee, Rohrer, and Sparks, 1988) to the posterior parietal cortex in the monkey encoding our representation of space (Pouget and Sejnowski, 1997).

Correlation population codes exploit the exact temporal relationships among streams of action potentials. One way to discover such codes is to record from two or more neurons simultaneously and to measure their cross-correlation function. For instance, it may be that two presynaptic neurons always generate spikes within 1 or 2 msec of each other. Much technological advance has occurred in this area in recent years, so that multi-unit recordings have now become routine.

In a variety of sensory systems in both invertebrates and vertebrates, physiological evidence indicates that cross correlations among groups of cells appear to encode various stimulus features (Freeman, 1975; Abeles, 1982a, 1990; Strehler and Lestienne, 1986; Eckhorn et al., 1988; Gray et al., 1989; Bialek et al., 1991; Eskandar, Richmond, and Optican, 1992; Konishi, 1992; Singer and Gray, 1995; Decharms and Merzenich, 1996; Wehr and Laurent, 1996). The best evidence to date linking neuronal synchronization directly to behavior comes from the bee's olfactory system (Stopfer et al., 1997). When pharmacological agents were used to block cellular synchronization—without interrupting neuronal activity *per se*—fine olfactory discrimination was disrupted.

Much theoretical work using pulse-coded neural networks has focused on the idea that spike coincidence across neurons encodes information (Sejnowski, 1977a; Abeles, 1982a, 1990; Amit and Tsodyks, 1991; Koch and Schuster, 1992; Griniasty, Tsodyks, and Amit, 1993; Abbott and van Vreeswijk, 1993; Zipser et al., 1993; Softky, 1995; Hopfield, 1995; Maass, 1996; van Vreeswijk and Sompolinsky, 1996). Indeed, it has been proposed that the precise temporal correlation among groups of neurons is a crucial signal for a number of perceptual processes, including figure-ground segregation and the binding of different attributes of an object into a single coherent percept (Milner, 1974; von der Malsburg, 1981; von der Malsburg and Schneider, 1986), selective visual attention (Niebur and Koch, 1994), and even the neuronal basis of awareness (Crick and Koch, 1990; for a review see Koch, 1993).

From our point of view as biophysicists, a correlation population code based on coincidence detection has the significant advantage that it is straightforward to implement at the membrane level (witness Fig. 21.2).

The question of rate versus correlation coding remains with us. Yet this stark either-or dichotomy is not very useful. Clearly, the timing of spikes, at least at the 10 msec level, is important. And in some systems, detailed information across groups of cells will also prove to be of relevance, although for which properties and at what time scale is an open question.

It therefore behooves us to study how accurately and reliably neurons can generate individual action potentials and how robust these are to noise. We here lay the groundwork by

introducing pulse neurons as well as firing rate models and describing their basic properties. We believe that such single-cell models represent the most reasonable tradeoff between simplicity and faithfulness to key neuronal attributes. The following chapter will deepen our discussion of stochastic aspects of neuronal firing. We will also discuss firing rate models.

14.2 Integrate-and-Fire Models

We turn to a very simple, but quite powerful model of a spiking cell with a long and distinguished history, first investigated by Lapicque (1907, 1926) before anything specific was known about the mechanisms underlying impulse generation. In its vanilla flavored version, it is known as the *integrate-and-fire* model (Stein, 1967a,b; Knight, 1972a; Jack, Noble, and Tsien, 1975; Tuckwell, 1988b; frequently also referred to as *voltage threshold* or *Lapicque's* model in the older literature). Its simplicity rivals physics' linear oscillator model, yet it does encapture the two key aspects of neuronal excitability: a passive, integrating subthreshold domain and the generation of stereotypical impulses once a threshold has been exceeded.

In the world of high speed electronics, integrate-and-fire models have their counterpart in the class of one-bit analog-digital converters known as *oversampled Delta-Sigma modulators* (Wong and Gray, 1990; Aziz, Sorensen, and van der Spiegel, 1996).[2]

The *nonleaky* or *perfect integrate-and-fire* unit consists but of a single capacitance for integrating the charge delivered by synaptic input in addition to a fixed and stationary voltage threshold V_{th} for spike initiation (Fig. 14.2). The *leaky* or *forgetful integrate-and-fire* model includes a resistance, accounting for leakage currents through the membrane. While integrate-and-fire models do not incorporate the detailed time course of the action potential, the effect of adaptation can be included. Indeed, the current-frequency relationship of such an integrate-and-fire cell with a handful of parameters can be very close to that of a much more complex, conductance-based cell model.

14.2.1 Perfect or Nonleaky Integrate-and-Fire Unit

We will be considering a number of variants of integrate-and-fire "units." All are characterized by a subthreshold domain of operation and a voltage threshold V_{th} for spike generation. The perfect integrate-and-fire unit deals with subthreshold integration via a single capacitance C. While unphysiological, it is mathematically tractable, which is why it is frequently invoked for pedagogical purposes. For the sake of mathematical convenience we assume the input to be a current $I(t)$, arising either from synaptic input or from an intracellular electrode. The generalization to a conductance-based input is straightforward.

The voltage trajectory of the perfect integrator is governed by the first-order differential equation

$$C\frac{dV(t)}{dt} = I(t)\,. \tag{14.3}$$

Together with an initial condition Eq. 14.3 specifies the subthreshold time course of the membrane potential.

Once the potential reaches V_{th}, a pulse is triggered and the charge that has accumulated on the capacitance is shunted to zero (through the open switch in Fig. 14.2A). This would normally be accomplished by the various conductances underlying spiking. Sweeping the

2. A significant body of mathematics has sprung up around these $\Delta\Sigma$ modulators that should be explored for its relevance to neuroscience; see, for example Norsworthy, Schreier, and Temes (1996).

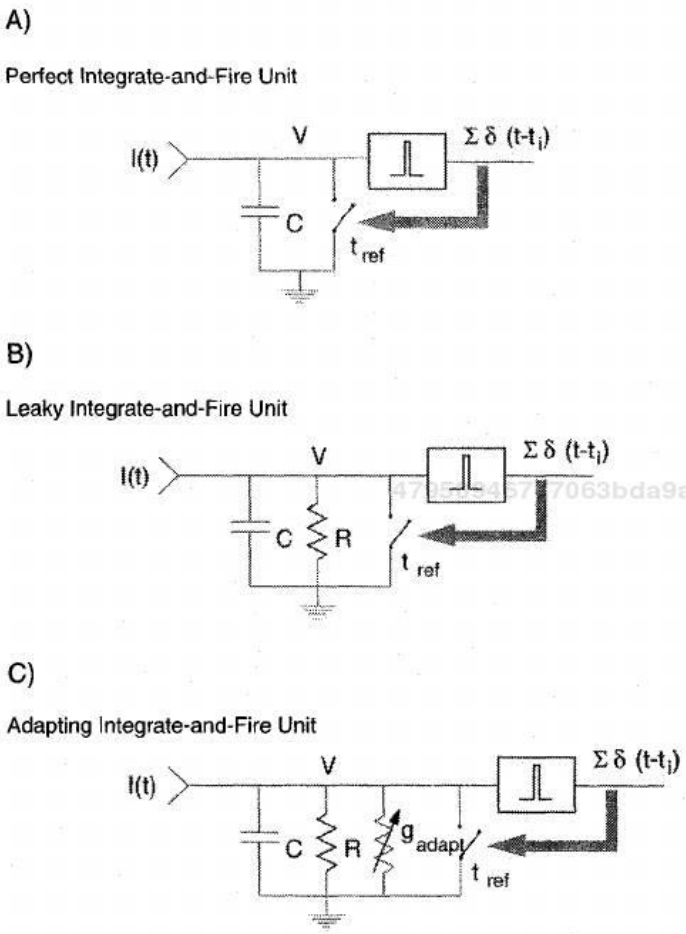

Fig. 14.2 INTEGRATE-AND-FIRE MODELS Three basic variants of integrate-and-fire units. Common to all are passive integration within a single compartment for the subthreshold domain and spike generation accomplished with a voltage threshold V_{th}. Whenever the membrane potential $V(t)$ reaches V_{th}, a pulse is generated and the unit is short-circuited. For a duration t_{ref} following spike generation, any input $I(t)$ is shunted to ground (corresponding to an absolute refractory period). **(A)** The *perfect* or *nonleaky* integrate-and-fire model contains but a capacitance. **(B)** The *leaky* or *forgetful* integrate-and-fire unit accounts for the decay of the membrane potential by an additional component, a leak resistance R. **(C)** The *adapting* integrate-and-fire unit with six free parameters (Eqs. 14.12 and 14.13) shows firing rate adaptation via the introduction of g_{adapt}, corresponding to a calcium-dependent potassium conductance (in addition to the absolute refractory period). Each spike increments the amplitude of the conductance; its value decays exponentially to zero between spikes.

charge to "ground" has the effect of instantaneously resetting $V(t)$ to zero. Because the model has no pretense of mimicking the currents involved in shaping the action potential, spike generation itself is not part of the model. Formally, we model the action potential by assuming that at the instant t' at which $V(t') = V_{\text{th}}$ (or the first time $V(t)$ exceeds V_{th} for models with instantaneously rising EPSPs) an output pulse, described by the delta function $\delta(t - t')$, is generated. The successive times t_i of spike occurrence are determined recursively from the equation

$$\int_{t_i}^{t_{i+1}} I(t)dt = CV_{\text{th}}\,. \tag{14.4}$$

As discussed in section 6.4, a canonical way in which experimentalists characterize a cell's behavior is by determining its *discharge* or f–I curve, the relationship between the amplitude of an injected current step and the average firing frequency (defined over an interval longer than the interspike interval; as in Eq. 14.1, $\langle f \rangle$ is computed as the inverse of the interspike interval).

In response to a sustained current, the membrane potential will charge up the capacitance until V_{th} is reached and V is reset to zero. The larger the current, the smaller the intervals between spikes and the higher the firing rate, according to

$$\langle f \rangle = \frac{I}{CV_{th}}. \tag{14.5}$$

Three features are worthwhile here. (1) The firing rate is linearly related to the input current (Fig. 14.3B). (2) Arbitrarily small input currents will eventually lead to a spike, since no input is forgotten. (3) The output spike train is perfectly regular. Of course, real neurons rarely, if ever, respond to a sustained current injection with a regular discharge of spikes but instead show substantial variability in the exact timing of the spikes. This is particularly true of neurons recorded *in vivo* (Holt et al., 1996). The following chapter will deal with this situation.

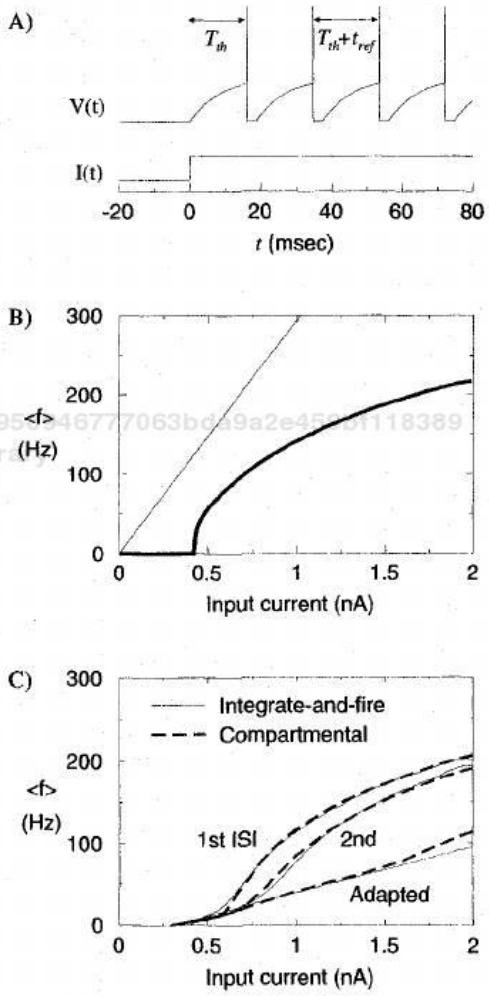

Fig. 14.3 SPIKING IN A LEAKY INTEGRATE-AND-FIRE MODEL Average firing frequency, determined as the inverse of the interspike interval, as a function of the amplitude of a maintained current input, for a leaky integrate-and-fire unit (Fig. 14.2B). **(A)** Exemplar trace of such a unit receiving a current step input with $I = 0.5$ nA. Before the membrane potential has time to reach equilibrium, the unit spikes. $V_{th} = 16.4$ mV, $C = 0.207$ nF, $R = 38.3$ MΩ, and $t_{ref} = 2.68$ msec. **(B)** f–I or *discharge* curve for the same leaky unit with refractory period (Eq. 14.11). The slope is infinite at threshold ($I_{th} = V_{th}/R$). The firing rate saturates at $1/t_{ref}$. For comparison, the f–I curve of the nonleaky unit without refractory period with constant slope $1/(V_{th}C)$ is superimposed. **(C)** An adapting conductance (with $G_{inc} = 20.4$ nS and $\tau_{adapt} = 52.3$ msec) is added to the leaky integrate-and-fire unit (see Fig. 14.2C) and the resulting f–I curve is compared against the discharge curve of the biophysical detailed compartmental model of the layer 5 pyramidal cell (Fig. 17.10). The degree of matching between simple and very complex models is quite remarkable and supports our contention that suitably modified integrate-and-fire models do mimic numerous aspects of the behavior of neurons. Adaptation is already evident when considering the first interspike interval (between the first and second spikes). Adaptation linearizes the very steep f–I curve around I_{th} (compare with B).

The dynamic firing range of nerve cells is limited by the fact that the sodium current responsible for spiking must recover from inactivation. Potassium currents furthermore limit the peak firing range. The effect of the absolute refractory period is mimicked by postulating that following spike generation, the membrane potential is set to zero for a fixed duration t_{ref}; any current arriving within this window is shunted away. This introduces a nonlinear saturation into the f–I curve of the perfect integrator,

$$\langle f \rangle = \frac{I}{C V_{th} + t_{ref} I} . \tag{14.6}$$

The output of such an integrator to an arbitrary input current consists of a series of impulses, $\sum_i \delta(t - t_i)$, all of which are spaced at least t_{ref} apart.

14.2.2 Forgetful or Leaky Integrate-and-Fire Unit

The model considered so far will sum linearly multiple subthreshold inputs irrespective of their temporal relationship because no account is made of a leak. A more realistic behavior is obtained by incorporating a leak resistance into the subthreshold domain (Fig. 14.2B),

$$C \frac{dV(t)}{dt} + \frac{V(t)}{R} = I(t) . \tag{14.7}$$

Having first met this equation in Chap. 1 (Eq. 1.5), we know that the evolution of the subthreshold voltage is completely characterized by convolving $I(t)$ with the associated Green's function, $e^{-t/\tau}$ (with $\tau = RC$). The time course of the membrane potential of the leaky integrate-and-fire unit to a step of constant current I, switched on at $t = 0$ and remaining on, can be obtained by solving Eq. 14.7,

$$V(t) = IR(1 - e^{-t/\tau}) + V(t = 0)e^{-t/\tau} . \tag{14.8}$$

The membrane charges exponentially up to its stationary value $V = IR$.

The integrator model will only follow this equation as long as the voltage remains below V_{th}, since upon reaching the threshold a spike is initiated and the voltage is reset to zero (Fig. 14.3A). The minimal sustained current necessary to trigger an action potential, that is, the threshold current, is

$$I_{th} = \frac{V_{th}}{R} . \tag{14.9}$$

For any current I larger than I_{th}, an output impulse will be generated at time T_{th}, such that $IR(1 - e^{-T_{th}/\tau}) = V_{th}$ holds. Inverting this relationship yields the time to spike as

$$T_{th} = -\tau \ell n \left(1 - \frac{V_{th}}{IR}\right) . \tag{14.10}$$

Solving this equation for the minimal duration needed for a sustained current of a fixed amplitude to generate a spike generates what is known as the *strength-duration curve* (Noble and Stein, 1966; Jack, Noble, and Tsien, 1975). Since the voltage is reset following an impulse and if we assume that the input current persists, the membrane will again charge up to the threshold, triggering the next spike $T_{th} + t_{ref}$ later (Fig. 14.3A).

If we take proper account of the refractory period by assuming that for t_{ref} following each spike all input current is simply lost (due to the shunting effect of the conductances underlying the afterhyperpolarization), the continuous firing rate as a function of the injected current will be (Fig. 14.3B)

$$\langle f \rangle = \frac{1}{T_{\text{th}} + t_{\text{ref}}} = \frac{1}{t_{\text{ref}} - \tau \ell n\,(1 - V_{\text{th}}/IR)}\,. \tag{14.11}$$

For currents below I_{th} no spike is triggered and at $I = I_{\text{th}}$, the slope of the f–I curve is infinite. For large currents, the firing rate saturates at the inverse of the refractory period (Fig. 14.3B). In the absence of a refractory period, the slope of the f–I curve levels off to a constant value of $1/(V_{\text{th}}C)$, identical to the slope of the nonleaky unit.[3] Its steepness can be increased by reducing the threshold voltage or by decreasing the membrane capacitance. Due to the refractory period, the f–I curve gently bends over to level off at $f_{\max} = 1/t_{\text{ref}}$ for (unphysiologically) high current levels.

14.2.3 Other Variants

Besides the generic version of the integrate-and-fire model discussed above, a number of variants are in use.

1. In order to better account for the 50–100 msec time course of adaptation, Wehmeier and colleagues (1989) introduced a purely time-dependent shunting conductance g_{adapt} (with a reversal potential equal to the resting potential, here assumed zero). Each spike increases this conductance by a fixed amount G_{inc}; between spikes, g_{adapt} decreases exponentially with a time constant τ_{adapt}. Such an effective calcium-dependent potassium conductance imitates both the absolute and the relative refractory period following spike initiation. We will refer to such a unit as an *adapting* integrate-and-fire model (Fig. 14.2C). Note that a refractory period t_{ref} is still necessary in order to mimic the very short-term aspect of adaptation. In the subthreshold domain, this unit is described by

$$C\frac{dV}{dt} = -\frac{V(1 + Rg_{\text{adapt}})}{R} + I \tag{14.12}$$

$$\tau_{\text{adapt}}\frac{dg_{\text{adapt}}}{dt} = -g_{\text{adapt}}\,. \tag{14.13}$$

   If V reaches V_{th} at time t', a spike is generated at this point in time and $g_{\text{adapt}}(t')$ is incremented by G_{inc}. This model is completely characterized by six parameters: V_{th}, C, R, t_{ref}, G_{inc} and τ_{adapt}.

2. An alternative to this output-dependent membrane conductance is to increase the voltage threshold following each spike in a deterministic manner, for instance, using the rule

$$V_{\text{th}}(t) = V_{\text{th},0}(1 + \alpha e^{-(t-t')/\tau_{\text{adapt}}})\,, \tag{14.14}$$

   where $t - t'$ is the time from the last impulse, $V_{\text{th},0}$ the threshold in the absence of any adaptation, and α the maximal normalized voltage threshold (Calvin and Stevens, 1968; Holden, 1976).

3. In order to account for those neurons that do not show any profound afterhyperpolarization following spiking, the membrane potential can be reset to a value closer to V_{th} (e.g., 20% of V_{th}) instead of zero. This is equivalent to resetting the potential to zero but adding a constant current and can have a considerable effect on the jitter in pulse timing (Troyer and Miller, 1997).

3. This can be seen upon developing the ℓn term in Eq. 14.11 into a Taylor series, with $\ell n(1 + x) \approx x - x^2/2$ for $|x| \ll 1$.

4. In a strategy to imitate the seemingly random nature of spike times, some authors resort to drawing the voltage threshold from some probability density distribution (Holden, 1976; Gestri, Masterbroek, and Zaagman, 1980). Yet in real neurons, the spiking mechanism itself appears to be quite reliable (Calvin and Stevens, 1968; Mainen and Sejnowski, 1995). In the case of the perfect integrator, a random threshold and a constant input can be shown to be equivalent to a random input and a constant threshold. Frequently, the former situation is both mathematically and computationally easier to deal with than the latter (for more details, see Gabbiani and Koch, 1998).

What all of these models share is a mechanism for passive integration of synaptic inputs, a voltage threshold for spike initiation, and a lack of specific spiking currents.

In Chap. 17 we will learn that an action potential in a full-blown model of a pyramidal cell (with eight voltage-dependent conductances) is, indeed, generated whenever the somatic membrane potential exceeds −49 mV. This is because the synaptic current flowing into the soma—caused by rapid EPSPs on the time scale of milliseconds—primarily charges up the capacitance. Relative to this rapid charging current, the ionic currents in the subthreshold regime change on a much slower time scale.

How well does this f–I curve compare against curves obtained from much more detailed and sophisticated models? Presaging Sec. 17.5, we plot the f–I curve of the layer 5 pyramidal cell, including the effect of firing rate adaptation, in Fig. 14.3C. Notice the very low slope of the f–I curve around threshold, in contrast to the infinite slope of the f–I curve of the leaky integrate-and-fire unit. If an adapting conductance is incorporated into the leaky integrator (Eqs. 14.12 and 14.13 and Fig. 14.2C), it is surprising how well this single-cell model (with just six degrees of freedom) resembles the much more detailed compartmental model based on membrane conductances.

Due to the presence of the leak term, integrate-and-fire models have been difficult to fully characterize analytically but have also been surprisingly successful in describing neuronal excitability. They have been applied to model the firing behavior of numerous cell types: neurons in the limulus eye (Knight, 1972b), α motoneurons (Calvin and Stevens, 1968), neurons in the visual system of the housefly (Gestri, Masterbroek and Zaagman, 1980), cortical cells (Softky and Koch, 1993; Troyer and Miller, 1997), and others.

While singing the praise of integrator models, it must be pointed out that many cells do not behave like integrate-and-fire units. For instance, cerebellar Purkinje cells (Jaeger, DeSchutter, and Bower, 1997) or the many types of oscillating neurons that constitute the central pattern generators found throughout the animal kingdom (Marder and Calabrese, 1996) have such strong inherent nonlinearities, generated by powerful intrinsic currents, that any attempts to directly map their behavior onto this class of models would fail miserably. Approximations are possible, though. For instance, bursting (Chap. 16) could be treated by letting the rapid Na^+ spikes be handled by the integrate-and-fire threshold mechanism. The slow dynamics governing at what instant the burst is triggered are generated by incorporating voltage-dependent conductances into the unit.

14.2.4 Response Time of Integrate-and-Fire Units

When a spiking, nonadapting membrane (such as the squid axon) receives a sustained suprathreshold current input, its membrane potential never reaches an equilibrium but moves along a limit cycle. That is, it undergoes periodic changes in its state variables (Chap. 7). When the integrate-and-fire neuron spikes, and the state variable is reset, it loses memory of the previous input current and begins to respond to the new current by charging toward the

threshold. It follows from these considerations that if there is a step change in current, the integrate-and-fire neuron must converge to its limit cycle by the end of the *first* interspike interval after the change, because everything during this first interval is exactly the same as during subsequent intervals.

Figure 14.4 compares the step response of an integrate-and-fire unit, a compartmental model of a cortical pyramidal neuron, an experimental record derived from a neuron in cat visual cortex, and a mean-rate neuron. The first interspike interval already reflects the new firing rate—the convergence occurs on as short a time interval as can be defined (that is, the interspike interval). The inclusion of adaptation currents (Fig. 14.3B) does not substantially affect this analysis. Cortical cells (Fig. 14.4C) also reach their maximum firing rate by the first interspike interval. Thereafter, the firing rate decreases slowly due to the temporal dynamics of adaptation.

Just because the subthreshold dynamics are governed by τ does not imply that the neuron must respond to a suprathreshold input with the same dynamics. Returning to expression 14.10 for the time to spike T_{th}, we notice that the larger the injected current, the sooner the cell spikes (Fig. 14.5A). Furthermore, T_{th} actually decreases as the input resistance, and therefore τ increases (Fig. 14.5B). This can easily be explained by recalling that T_{th} is the time it takes for the membrane potential to reach the fixed threshold V_{th}. Increasing the input resistance will shorten this time, even if overall it would have taken the membrane longer to reach its ultimate steady-state value RI (which is never reached since a spike is triggered and the membrane potential reset once V hits V_{th}).

14.3 Firing Rate Models

The potential in a continuous firing rate unit, such as those at the heart of most neural networks, has the same dynamics as that in the leaky integrate-and-fire unit,

$$C\frac{dV(t)}{dt} = -\frac{V(t)}{R} + I(t)\,. \tag{14.15}$$

A subtle but far-reaching difference is that the instantaneous output of this unit $f(t)$ is a continuous but nonlinear function of $V(t)$:

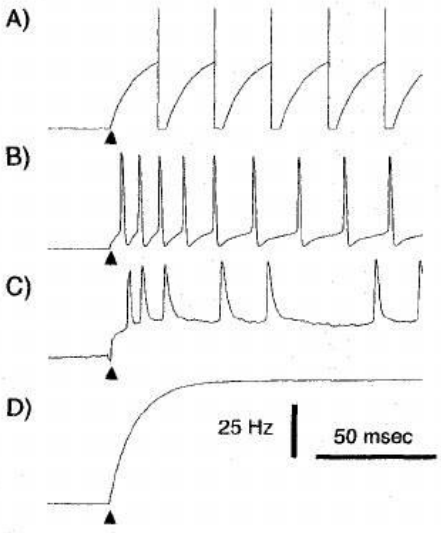

Fig. 14.4 SPIKING CELLS Sample spike rasters in response to a step current injection. **(A)** Leaky integrate-and-fire unit with refractory period spiking in response to a current step of 1.6 nA (for parameters, see legend to Fig. 14.3A). The arrows indicate the time at which the current injection commenced. **(B)** Somatic membrane potential in the layer 5 pyramidal cell model in response to a 1.5-nA current input. **(C)** Response of a cell in the primary visual cortex of the anesthetized adult cat to a 0.6-nA current injection (from Ahmed et al., 1993). The firing rate does not increase gradually; the effect of the change in current is fully visible in the first interspike interval. **(D)** Output of a nonadapting firing rate model with $\tau = 20$ msec. In the linear regime of the cell's f–I curve, the firing rate can be considered to be a low-pass-filtered version of the step input.